RSC Advances

ROYAL SOCIETY OF CHEMISTRY

www.rsc.org/advances

Heptazine-based graphitic carbon nitride as an effective hydrogen purification membrane

Yujin Ji[1], Huilong Dong[1], Haiping Lin [1,*], Liling Zhang[1],Tingjun Hou[1], Youyong Li [1,*]

1 Institute of Functional Nano & Soft Materials (FUNSOM), Jiangsu Key Laboratory for Carbon-Based Functional Materials & Devices, Soochow University, Suzhou, Jiangsu 215123, China

[*] Corresponding author. E-mail: yyli@suda.edu.cn (Youyong Li), hplin@suda.edu.cn (Haipin Lin)

Abstract The purification of H_2 from other gases (CH_4, CO, CO_2, N_2, and H_2O) is a vital step for its safe usage. By using the first-principles calculations and molecular dynamics simulations, we find that the porous graphitic carbon nitride (g-C_3N_4) monolayer works as an efficient and highly selective hydrogen purification membrane. In the DFT calculations, the transition state theory is used to search the lowest diffusion barrier (0.55eV) for H_2 to go through the well-ordered intrinsic holes. Meanwhile, the excellent selectivity between H_2 and other gases shows that the g-C_3N_4 nanosheet is specific for diffusion of H_2. The MD simulations exhibit the whole dynamic purification processes and confirm our previous DFT results. Our results indicate that the g-C_3N_4 nanosheet has great potential in separating H_2 from undesirable gases.

1. Introduction

Hydrogen, as an environment-friendly, sustainable and high-energy-density resource, is regarded as one of the most efficient substitutes of fossil fuels to address the issue on the shortage of energy in the future.[1, 2] However, a technical challenge in hydrogen production, storage, transportation and usage is the existing of undesirable gases, which may result in security risks. For example, a mixture of H_2, CO, and CH_4 is produced through the steam-methane reforming in current hydrogen production method.[3] The purification of H_2 from undesirable gases (CH_4, CO, CO_2, N_2, and H_2O) is, therefore, regarded as an important step in the hydrogen production process. Compared with traditional gas separation techniques (e.g. pressure swing adsorption or cryogenic distillation), two-dimensional (2D) materials with single-atom thickness seem more promising because of their distinct advantages in the low energy consumption and recycling through the physical interaction at the atomistic scale.[4, 5]

The search and design of appropriate porous 2D materials have attracted wide attention both by theoretical calculations and experimental investigations.[6-9] In general, a suitable H_2 purification membrane should possess two characteristics: a) no/little interaction between H_2 and membrane materials; b) a certain diffusion barrier to differentiate migration between H_2 and other gases migration. Correspondingly, the permeance and selectivity are two important factors to evaluate the performance of purification membrane.[10] Organic 2D materials including carbon-based[11, 12], polymer[13] and h-BN membranes[14, 15] and inorganic materials[16] containing metallic, silica[17] and zeolite[18] membranes are current well-known membrane materials. Notably, Jiang et al[19] demonstrated that porous graphene with hydrogenated and nitrogen-functionalized at the edge of pores can facilitate H_2/CH_4 separation and reduce the barrier for H_2 diffusion. Meanwhile, the doping of nitrogen atom

will not modify the hydrogen adsorption ability. Thus, it is straightforward for us to consider 2D carbon nitride material as a natural membrane in the H_2 purification and filtering.

Graphitic carbon nitride (g-C_3N_4) is similar to graphene with a sp^2 π-conjugated system through van der Waals interaction between layers, which has been applied in the field of energy and materials science.[2, 20-24] Free-standing g-C_3N_4 monolayer is chemically and thermally stable. It can be synthesized by the thermal polycondensation process[2] and have shown huge potentials in the spintronic devices[25] and photocatalysis fields[26, 27]. The single layer g-C_3N_4 is a direct band gap of about 2.4eV at the gamma point, rendering them promising as metal-free water-splitting materials. At the same time, the intrinsic vacancies surrounded with nitrogen atoms in g-C_3N_4 nanosheet provide natural pathways for gases to diffuse compared to the extra/man-made pores or defects in other 2D materials, which makes them promising for H_2 purification.

In this context, we report that the g-C_3N_4 nanosheet may serve as an effective and highly selective H_2 separation membrane *via* the first principles calculations. The target mixtures include H_2/ (CH_4, CO) from the steam-methane reforming, H_2/H_2O from water splitting. The size of the intrinsic hole in g-C_3N_4 is an appropriate, well-ordered pore and exhibits a higher permeability and selectivity for H_2 rather than H_2O, N_2, CO, CO_2, and CH_4. The combination of g-C_3N_4 in catalytic water splitting and H_2 purification will greatly extend the practical applications of g-C_3N_4 materials.

2. Computational details

First, all of the first principles calculations were carried out by the Vienna Ab-initio Simulation Package (VASP)[28]. The Perdew-Burke-Ernzerhof (PBE)[29] functional with van der Waals correction (DFT-D2)[30] was chosen to consider the

interaction between the gas molecules and g-C_3N_4. The climbing image nudged elastic band (CI-NEB) method[31] was used to search the minimum energy pathway (MEP) when gases diffuse through the porous g-C_3N_4. The cut-off energy was set to 500 eV and the surface Brillouin zone was sampled with 5×5×1 Monkhorst-Pack k-point grids. A vacuum thickness of 20 Å with periodic boundary conditions was set to avoid the interactions between periodically-repeated layers. All of the structural relaxations are accomplished until the energy change is less than 10^{-4} eV and force change is less than 0.001 eV/Å. The adsorption energy (E_a) between gases and g-C_3N_4 is defined as

$$E_a = E_{gas@g-C_3N_4} - (E_{gas} + E_{g-C_3N_4})$$

where $E_{gas@g-C_3N_4}$, E_{gas} and $E_{g-C_3N_4}$ are the total energy of a gas molecule adsorbed on g-C_3N_4, a single gas molecule and g-C_3N_4 respectively. It should be noted that specific adopted functional plays a role on the calculation of gas permeation barriers because of the effect of short/long-range[32, 33] force at the quantitative level, but it will not influence the qualitative permeation trend[34].

Then the MD simulations of H_2, N_2, H_2O, CO, CO_2 and CH_4 permeation were implemented by Forcite module available in Materials Studio software package. Similar as previous work[12, 14, 35], gas molecules were interspersed between the g-C_3N_4 membranes and the initial conditions were 300 K with a total time of 1000 ps. The constant-volume and constant-temperature (NVT) ensemble and COMPASS[36] forcefield were employed during the simulation with a time step of 1fs. The electrostatic interaction and van der Waals interaction were calculated using the atom based method.

3. Results and discussion

The geometric structure of g-C_3N_4 is determined first. Unlike the planar graphene, the single layered g-C_3N_4 forms two configurations - planar and buckled structures, containing 6 carbon and 8 nitrogen atoms in the primitive unit cell, as shown in Figure 1. The optimized lattice constant of the planar

g-C_3N_4 is 7.13 Å, in good agreement with the previous investigation[2] and the lattice constant of the buckled one is calculated to be 7.05 Å. When gas molecules adsorb on the surface of planar g-C_3N_4, the planar one transforms into the buckled one and this transformation is irreversible. Moreover, the buckled unit cell is 0.50 eV per unit cell more stable than the planar one, indicating a higher stability. This agrees well with previous reports.[37] The more stable buckled structure is, therefore, adopted for the following studies. Our buckled configuration is more stable than the reported planar graphitic carbon nitride[38], which has a better H_2 purification performance.

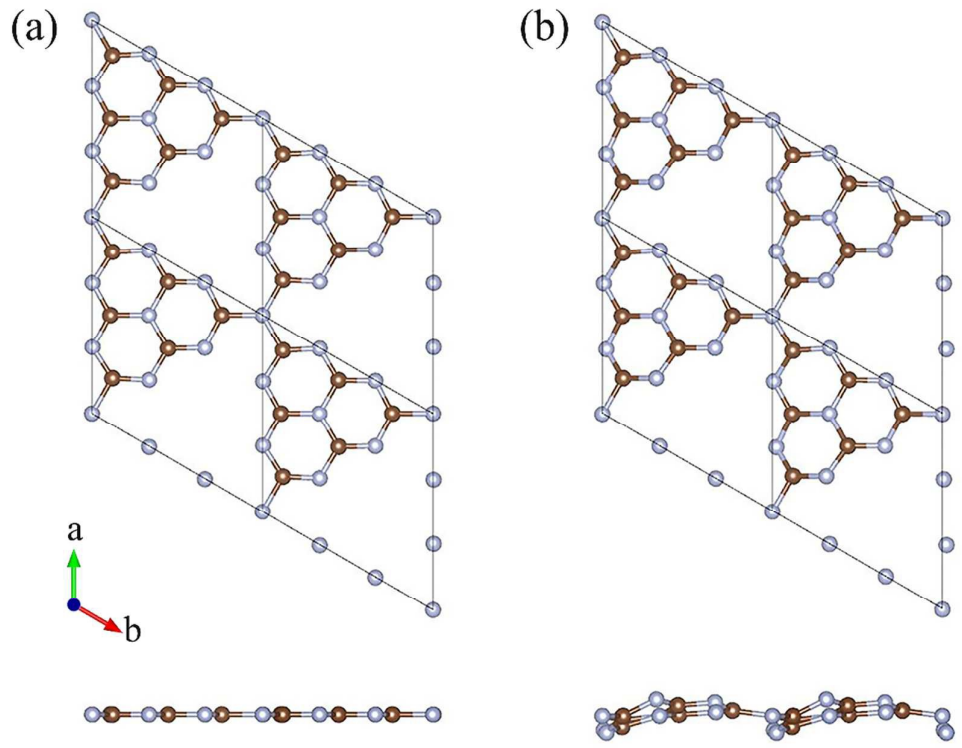

Figure 1. Schematic illustrations of 2×2 g-C_3N_4 (top view and side view) supercells: (a) the planar g-C_3N_4 and (b) the buckled g-C_3N_4. The nitrogen and carbon atoms are represented by the blue beads and grey beads, respectively.

Then various gas molecules (containing H_2, H_2O, N_2, CO, CO_2, and CH_4) adsorbed on the g-C_3N_4 with different adsorption configurations are

investigated. Our simulations demonstrate that the adsorption sites of H_2, H_2O, N_2, CO, and CO_2 are at the intrinsic vacancy of g-C_3N_4 while the CH_4 prefers to adsorb above the hexagonal ring (the equilibrium adsorption configurations are presented in Figure 2). The equilibrium adsorption heights and energies are summarized in Table 1. As listed in Table 1, the calculated equilibrium distance between molecules and substrate is mostly within 2~3 Å. The adsorption energies of most gas molecules are smaller than 0.3 eV, which indicates that the common adsorption mode is physisorption through weak van der Waals (vdW) interaction. H_2O molecule is an exception because of the orbital hybridization between H_2O and g-C_3N_4 nanosheet, which results in a much higher adsorption energy (the comparison between the density of state of H_2O absorbed g-C_3N_4 and pure buckled g-C_3N_4 is shown in Figure. S1 of Supplementary Data). It is worth noting that the adsorption configuration of H_2 here is similar with the pristine and nitrogen-doped graphdiyne[9, 39], confirming that the nitrogen atoms negligibly affect the adsorption properties.

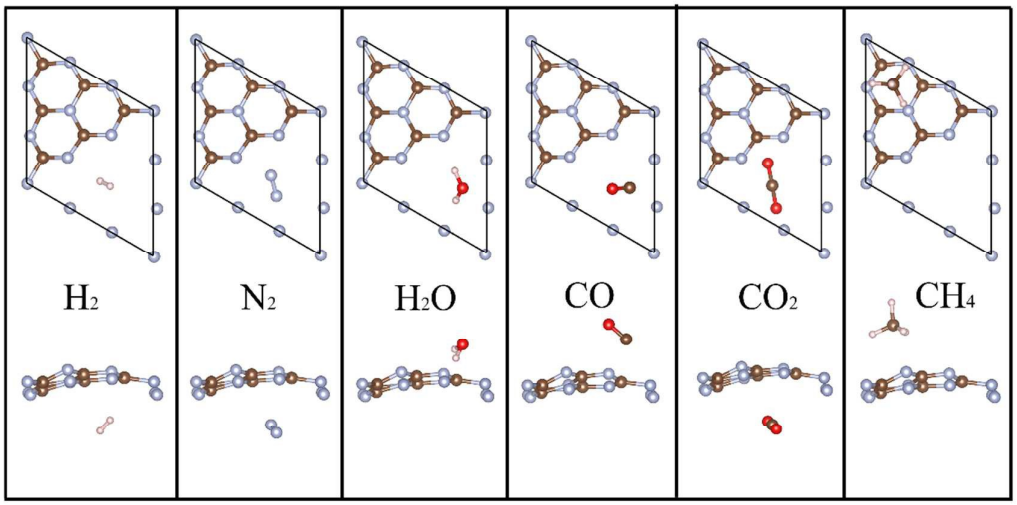

Figure 2. The equilibrium adsorption configuration of H_2, N_2, H_2O, CO, CO_2 and CH_4. The blue beads, grey, white and red beads represent the nitrogen, carbon, hydrogen, and oxygen atoms respectively (top view and side view).

Table 1. The equilibrium adsorption heights (D_0), adsorption energies (E_a) and diffusion barriers (E_b) of H_2, H_2O, N_2, CO, CO_2, and CH_4 molecules.

	D_0 (Å)	E_a(eV)	E_b(eV)
H_2	2.68	-0.078	0.55
H_2O	1.07	-0.513	1.59
N_2	2.87	-0.117	1.95
CO	2.03	-0.155	1.80
CO_2	2.93	-0.226	1.50
CH_4	2.31	-0.163	3.36

Next, in order to investigate the process of gas molecules passing through a g-C_3N_4 nanosheet, the initial state (IS) of the H_2 molecule is set as that the H-H axis is perpendicular to the plane with a distance of nearly 5Å between H_2 and the centre of a vacancy in g-C_3N_4 nanosheet. The diffusion energy barrier is given by

$$E_b = E_{TS} - E_{SS}$$

where E_{TS} and E_{SS} represent the total energy of the transition state (TS) and the most stable state (SS) of H_2 when permeates through the porous g-C_3N_4 nanosheet. The energy profiles of diffusion pathways for different gas molecules are plotted in Figure 3 and the diffusion energy barriers (E_b) are listed in Table 1. The H_2 diffusion barrier is about 0.55 eV, which is significantly higher than that of nitrogen-doped graphdiyne (0.08 eV)[39] and silicene with 585-divacancy (0.34eV)[40] but is sufficiently surmountable at moderate temperature and pressure. Meanwhile, the calculated diffusion energy

barriers are 1.50 eV, 1.59 eV, 1.80 eV, and 1.95 eV for CO_2, H_2O, CO and N_2, respectively. Obviously, the high E_a for H_2O molecule makes it difficult to pass through the g-C_3N_4 nanosheet. At the same time, it is worth noting that the diffusion energy barrier for CH_4 is 3.36 eV, showing that it is extremely difficult for CH_4 to permeate the intrinsic vacancy of g-C_3N_4 nanosheet. Therefore, it is predicted that the g-C_3N_4 can work as an ideal hydrogen purification membrane with high selectivity, especially for separation of H_2/CH_4 mixture.

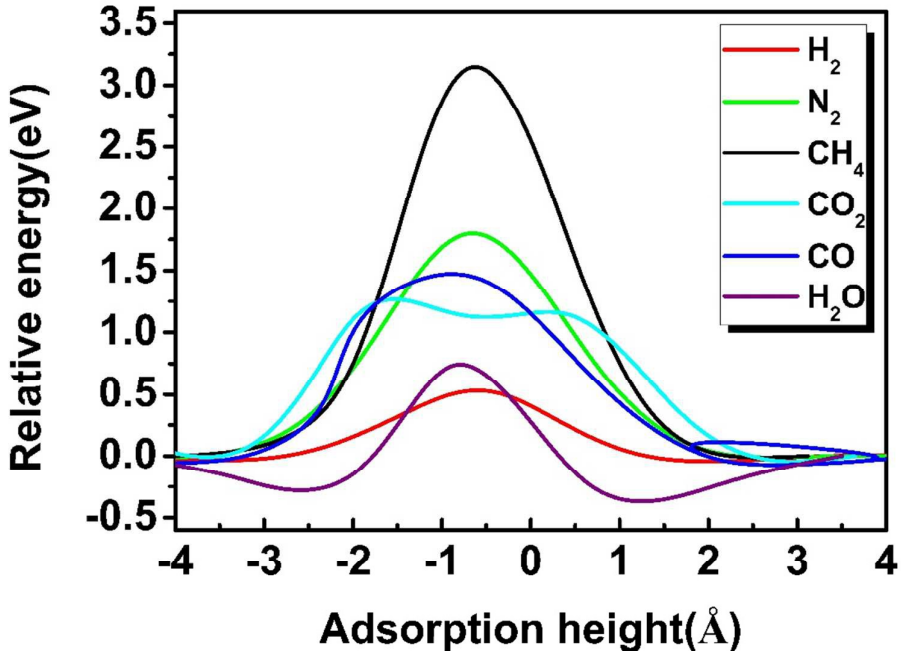

Figure 3. (a) Minimum energy pathways for H_2, H_2O, N_2, CO, CO_2, and CH_4 molecules passing through g-C_3N_4.

Based on the MEP and diffusion energy barriers, we calculated the selectivity S and permeance P of various gas molecules to elucidate the properties of gas separation and diffusion for g-C_3N_4 nanosheet. For the

selectivity of H_2 with other gas molecules, it is calculated by using the following equation:[40, 41]

$$S_{H_2/r_{Gas}} = \frac{r_{H_2}}{r_{Gas}} = \frac{A_{H_2}\exp\{-E_{H_2}/k_BT\}}{A_{Gas}\exp\{-E_{Gas}/k_BT\}}$$

where A is the ideal gas diffusion prefactor, E_{Gas} is the diffusion energy barrier for different gas molecules (as listed in Table 1), k_B is the Boltzmann constant and T is the temperature. Here we assumed that the diffusion prefactors of H_2, H_2O, N_2, CO, CO_2, and CH_4 have the same value, the temperature-dependent selectivity are illustrated in Figure 4(a). The g-C_3N_4 nanosheet exhibits an excellent selectivity of H_2/CH_4 with 10^{46} at the room temperature (300K), much higher than those of H_2/H_2O (10^{17}), H_2/CO (10^{20}), H_2/CO_2 (10^{15}) and H_2/N_2 (10^{23}), showing an enormous advantage in H_2/CH_4 purification. This property is significantly superior to the similar 2D materials (shown at the Table 2). Then the classical permeance of gas molecules through membrane, defined as the ratio of the measured gases molar flux F (mol m^{-2} s^{-1}) to the difference of partial pressure Δp (Pa), is estimated by the following formula:[14, 41]

$$\mathrm{P} = \frac{F}{\Delta p} = \frac{p\int_{v_B}^{\infty} f(v)dv}{N_A\sqrt{2\pi \mathrm{m} k_B T}\Delta p}$$

where p, N_A, m, k_B and T represent the pressure, Avogadro constant, mass of molecule, Boltzmann constant and temperature, respectively. $f(v)$ denotes the Maxwell distribution, and the kinetic energy at v_B can overcome the barrier. Here we adopt an approximation that the feed gas on one side is at 1 bar and the other side of the membrane is filled with any other gas at 2 bar pressure as previous works[41]. Figure 4(b) shows that the permeance of different gas molecules increased with the temperature. The calculated permeance of H_2 across the g-C_3N_4 nanosheet at 300 K is 10^{-7}, which is acceptable for the industrial separation[42]. Thus our DFT results provide a solid proof that the

g-C_3N_4 with well-ordered pores is a potential H_2 purification membrane at the ambient atmosphere.

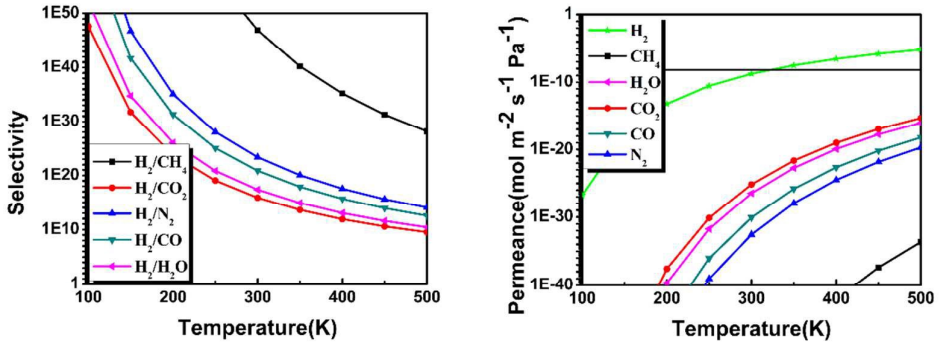

Figure 4. (a) selectivity and (b) permeance for H_2, H_2O, N_2, CO, CO_2, and CH_4 molecules passing through g-C_3N_4 nanosheet as a function of adsorption height or temperature. The horizontal line in the panel (b) is the industrial standard for gas permeation.[42]

Table 2. The diameter of the pore, the calculated H_2 adsorption energy, permeation barrier and selectivity of g-C_3N_4, H-graphene, graphdiyne and silicene.

Membrane	g-C_3N_4	H-graphene	Graphdiyne	Silicene
D_c(Å)	1.70	2.5	2.24	4.7
E_a(eV)	-0.078	-0.05	-0.07	-0.06
E_b(eV)	0.55	0.22	0.01	0.34
S(H_2/CH_4)	10^{46}	10^{23}	10^{10}	10^{22}

The N atoms at the edge of porous graphene can increase the electrostatic interaction compared to no edge-modified graphene, resulting in a better selectivity and permeability for gas molecules.[43, 44] To investigate the origin of such selectivity, we plotted the electron density distribution of different gas molecules permeating through the g-C_3N_4 at the transitional state structures in Figure 4. The distribution of electron density gives a way to describe the

interaction between the gas molecules and the substrate. Our results show that there is little electron density overlapping at the TS of H_2 diffusion compared with other TS configurations, suggesting that the electrostatic interaction plays a vital role during the permeation process. The electrostatic interaction will limit the permeation of other gas molecules due to the larger atomic sizes. Meanwhile, we plotted the vdW surface of g-C_3N_4 and gas molecules as shown in Figure 5. The pore size of the g-C_3N_4 (unoccupied by vdW surface) as well as the diameters of cross section (D_c, vdW occupied) of different gas molecules is also evaluated (the values are listed in Table 3). The diameter of g-C_3N_4 pore is about 1.70 Å, significantly smaller than that of N-graphdiyne (2.24 Å), while the D_c(2.44 Å) of H_2 presents more overlapping with the vdW surface of g-C_3N_4 pore. The comparison between the sizes of vdW surface well explains why g-C_3N_4 presents higher diffusion energy barrier and better selectivity for H_2. Moreover, the overlapping between the vdW surface of g-C_3N_4 and other gases seems too much for gas molecules to permeate. Therefore, the suitable size of intrinsic vacancy in g-C_3N_4 is not only favourable for H_2 diffusion but also helpful to hinder the permeation of other gas molecules. The N atoms at the rim of pores bring a strong electrostatic interaction and vdW interaction, resulting into excellent gas selectivity, which is consistent to previous analysis[43]. Additionally, different from the traditional pores or defects caused by dangling bonds, the nitrogen atoms at the rim of intrinsic vacancy of g-C_3N_4 are covalent bond with the nearby carbon atoms, which provides a more stable permeation environment for the gases diffusion.[19, 40] The good permeation of H_2 as well as the hindrance to other gases makes it feasible for application of g-C_3N_4 nanosheet in H_2 purification.

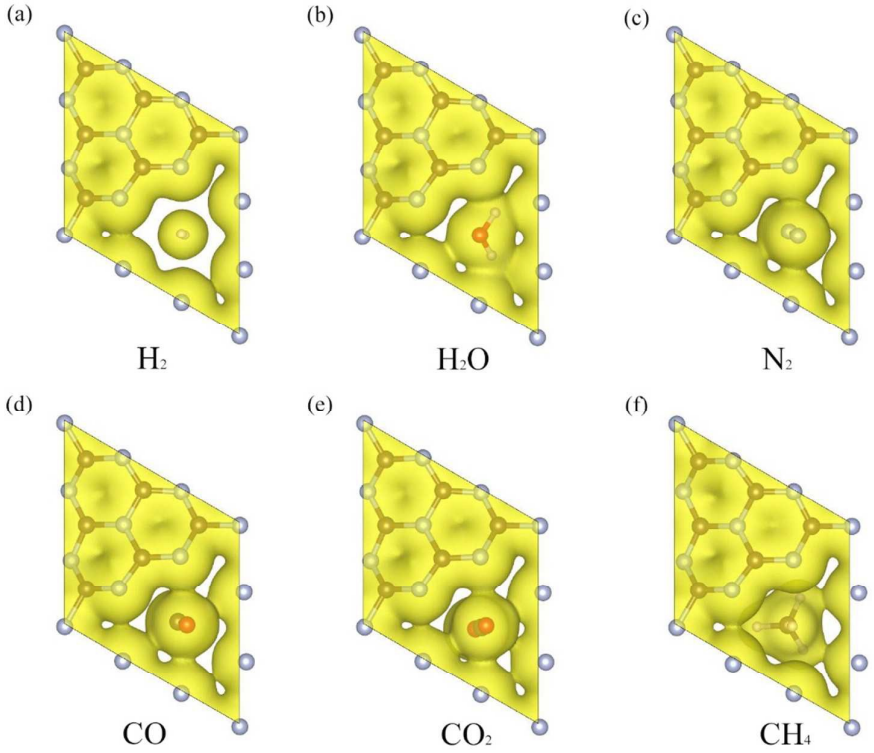

Figure 4. Electron density of (a) H_2 (b) H_2O (c) N_2 (d) CO (e) CO_2 and (f) CH_4 at their corresponding transition states. Isosurface value is 0.002 e/Å^3.

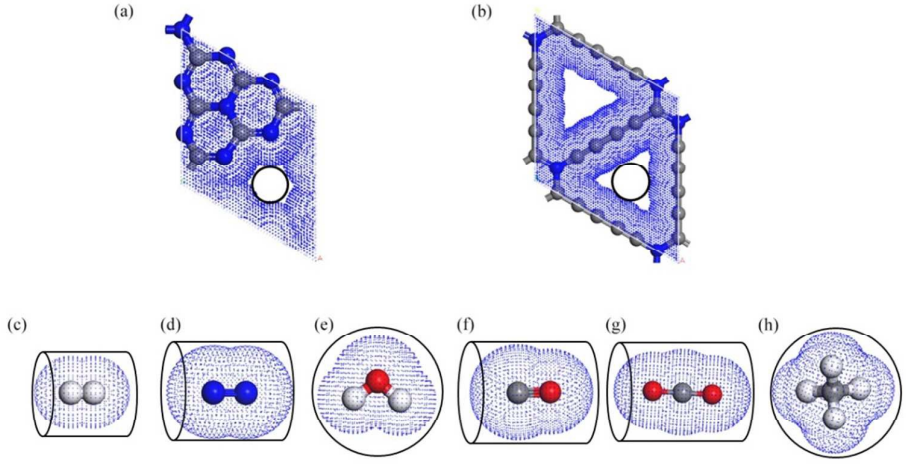

Figure 5 Geometric structure and van der Waals (vdW) surface of (a) g-C_3N_4

(b)N-graphdiyne[39] (c)H_2 (d)N_2 (e)H_2O (f)CO (g)CO_2 and (h)CH_4. The blue, grey, white and red beads represent the nitrogen, carbon, hydrogen, and oxygen atoms respectively.

Table 3 The vdW occupied a volume of H_2, N_2, H_2O, CO, CO_2 and CH_4 and their corresponding diameters of the cross section (D_c) of our sphere models.

	vdW occupied volume ($Å^{-3}$)	Diameter of cross section (Å)
H_2	10.87	2.44
N_2	23.76	3.20
H_2O	19.48	3.34
CO	26.90	3.46
CO_2	33.71	3.44
CH_4	28.41	3.78

In addition, we perform molecular dynamics (MD) simulations under the realistic condition to reproduce the dynamic process of H_2 and other gas molecules to diffuse through g-C_3N_4 nanosheet. A single component of 80 gas molecules and mixtures of 20 H_2, 20 N_2, 20 CO, 20 CO_2, 20 CH_4 and 20 H_2O gas molecules are put between the g-C_3N_4 nanosheets with a 1000ps MD simulation. The snapshot of pure 80 H_2 molecules and mixtures of 120 gas molecules at 0 ps, 500 ps, 1000 ps are given in Figure 6 (Single components of N_2, CO, CO_2, CH_4 and H_2O gas molecules is shown in the Figure S2). Therefore, we found that nearly 9 H_2 molecules diffuse through the g-C_3N_4 after 1000 ps MD simulation at the mixture system of 120 gas molecules. Meanwhile, it is difficult for other gas molecules to pass through the membrane at room temperature, which is consistent with our former DFT results and the mixtures of gas molecules do not influence the performance of H_2 purification. Other gas molecules are trapped between the membranes. The MD simulations reveal that the H_2 can escape from the intrinsic vacancies of g-C_3N_4 at the room temperature while other gases will be trapped on the one side of g-C_3N_4, which further confirms the reliability of our results from first principles calculations. Although it is difficult

for the experimenters to synthesize large-scale g-C_3N_4 nanosheets with well-order pores, it is still promising to be applied in small-size purification devices with the development of technology.

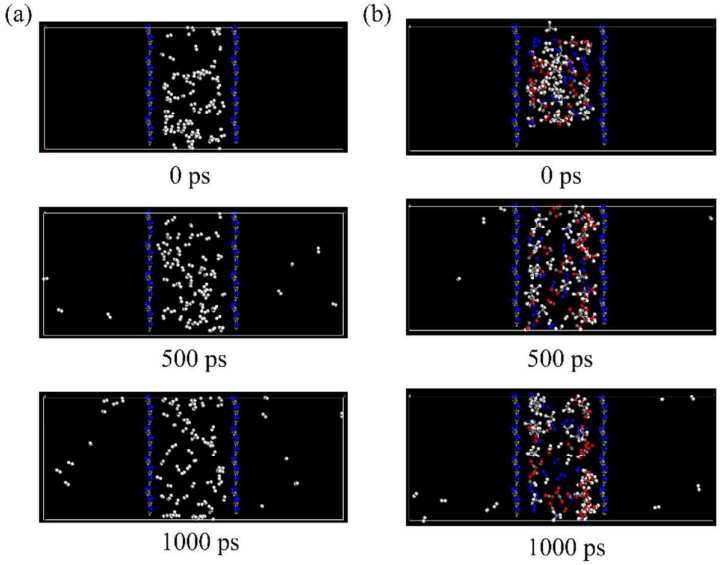

Figure 6. Snapshots of (a) H_2 (b) gas mixture permeating through g-C_3N_4 nanosheet in the 0~1000 ps MD simulation at 300 K. The blue, grey, white and red beads represent the nitrogen, carbon, hydrogen, and oxygen atoms respectively.

4. Conclusions

We have performed the feasibility analysis on g-C_3N_4 as H_2 purification membrane. The graphitic carbon nitride with well-ordered sized intrinsic vacancies offers potential diffusion pathways for hydrogen diffusion, which is superior to the graphene or silicene with extra/ man-made pores and defects. The minimum energy pathways determined by first principles calculations suggest that H_2 permeates the porous g-C_3N_4 with a surmountable diffusion barrier of 0.55 eV. Meanwhile, g-C_3N_4 exhibits a high selectivity between H_2 and other gases with the order of 10^{46} (H_2/CH_4) at the room temperature. Considering the good permeation of H_2 as well as the hindrance to other gases, we report that g-C_3N_4 may serve as a promising filtration membrane for H_2 purification. Our theoretical simulations provide an extra approach for the

application of g-C_3N_4 in addition to catalyzing water splitting into hydrogen.

Acknowledgement

The authors thank Dr. Yadong Zhang and Dr. Ruifeng Lu for valuable discussions and helps. The work is supported by the National Basic Research Program of China (973 Program, Grant No. 2012CB932400), the National Natural Science Foundation of China (Grant No. 21273158 and 21303112), the Natural Science Foundation of Jiangsu Province (Grant BK20130291), a Project Funded by the Priority Academic Program Development of Jiangsu Higher Education Institutions (PAPD). This is also a project supported by the Fund for Innovative Research Teams of Jiangsu Higher Education Institutions, Collaborative Innovation Center of Suzhou Nano Science and Technology.

References

1. M. Winter and R. J. Brodd, *Chem. Rev.*, 2004, **104**, 4245-4269.
2. X. C. Wang, K. Maeda, A. Thomas, K. Takanabe, G. Xin, J. M. Carlsson, K. Domen and M. Antonietti, *Nat. Mater.*, 2009, **8**, 76-80.
3. N. W. Ockwig and T. M. Nenoff, *Chem. Rev.*, 2007, **107**, 4078-4110.
4. M. Freemantle, *Chem. Eng. News*, 2005, **83**, 49-56.
5. W. G. Kim and S. Nair, *Chem. Eng. Sci.*, 2013, **104**, 908-924.
6. K. Y. Kang, B. I. Lee and J. S. Lee, *Carbon*, 2009, **47**, 1171-1180.
7. S. Giraudet, Z. H. Zhu, X. D. Yao and G. Q. Lu, *J. Phys. Chem. C*, 2010, **114**, 8639-8645.
8. S. W. Cranford and M. J. Buehler, *Nanoscale*, 2012, **4**, 4587-4593.
9. Y. Jiao, A. Du, M. Hankel, Z. Zhu, V. Rudolph and S. C. Smith, *Chem Commun*, 2011, **47**, 11843-11845.
10. H. Li, Z. N. Song, X. J. Zhang, Y. Huang, S. G. Li, Y. T. Mao, H. J. Ploehn, Y. Bao and M. Yu, *Science*, 2013, **342**, 95-98.
11. Y. Jiao, A. J. Du, M. Hankel and S. C. Smith, *Phys. Chem. Chem. Phys.*, 2013, **15**, 4832-4843.
12. L. W. Drahushuk and M. S. Strano, *Langmuir*, 2012, **28**, 16671-16678.
13. R. Lu, Z. Meng, D. Rao, Y. Wang, Q. Shi, Y. Zhang, E. Kan, C. Xiao and K. Deng, *Nanoscale*, 2014, **6**, 9960-9964.
14. Y. Zhang, Q. Shi, Y. Liu, Y. Wang, Z. Meng, C. Xiao, K. Deng, D. Rao and R.

Lu, *J Phys Chem C*, 2015, **119**, 19826-19831.
15. A. Nagashima, N. Tejima, Y. Gamou, T. Kawai and C. Oshima, *Phys. Rev. Lett.*, 1995, **75**, 3918-3921.
16. G. Q. Lu, J. C. D. da Costa, M. Duke, S. Giessler, R. Socolow, R. H. Williams and T. Kreutz, *J. Colloid Interface Sci.*, 2007, **314**, 589-603.
17. S. T. Oyama, D. Lee, P. Hacarlioglu and R. F. Saraf, *J. Membr. Sci.*, 2004, **244**, 45-53.
18. Y. Cui, H. Kita and K. Okamoto, *J. Mater. Chem.*, 2004, **14**, 924-932.
19. D. E. Jiang, V. R. Cooper and S. Dai, *Nano letters*, 2009, **9**, 4019-4024.
20. J. Zhang, Y. Chen and X. Wang, *Energy Environ. Sci.*, 2015.
21. J. Liu, H. Q. Wang, Z. P. Chen, H. Moehwald, S. Fiechter, R. van de Krol, L. P. Wen, L. Jiang and M. Antonietti, *Adv. Mater.*, 2015, **27**, 712-718.
22. A. Thomas, A. Fischer, F. Goettmann, M. Antonietti, J. O. Muller, R. Schlogl and J. M. Carlsson, *J. Mater. Chem.*, 2008, **18**, 4893-4908.
23. J. J. Zhu, P. Xiao, H. L. Li and S. A. C. Carabineiro, *ACS Appl. Mater. Interfaces*, 2014, **6**, 16449-16465.
24. X. C. Wang, K. Maeda, X. F. Chen, K. Takanabe, K. Domen, Y. D. Hou, X. Z. Fu and M. Antonietti, *J. Am. Chem. Soc.*, 2009, **131**, 1680-1681.
25. D. Ghosh, G. Periyasamy and S. K. Pati, *The Journal of Physical Chemistry C*, 2014, **118**, 15487-15494.
26. J. Liu, Y. Liu, N. Y. Liu, Y. Z. Han, X. Zhang, H. Huang, Y. Lifshitz, S. T. Lee, J. Zhong and Z. H. Kang, *Science*, 2015, **347**, 970-974.
27. Y. Wang, X. C. Wang and M. Antonietti, *Angew. Chem.-Int. Edit.*, 2012, **51**, 68-89.
28. G. Kresse and J. Hafner, *Phys. Rev. B*, 1993, **47**, 558-561.
29. J. P. Perdew, K. Burke and M. Ernzerhof, *Phys. Rev. Lett.*, 1996, **77**, 3865-3868.
30. S. Grimme, *J. Comput. Chem.*, 2006, **27**, 1787-1799.
31. G. Henkelman, B. P. Uberuaga and H. Jonsson, *J. Chem. Phys.*, 2000, **113**, 9901-9904.
32. A. Ambrosetti, A. M. Reilly, R. A. DiStasio, Jr. and A. Tkatchenko, *J. Chem. Phys.*, 2014, **140**, 18A508.
33. P. L. Silvestrelli and A. Ambrosetti, *J. Chem. Phys.*, 2014, **140**, 124107.
34. A. Ambrosetti and P. L. Silvestrelli, *J.Phys.Chem.C*, 2014, **118**, 19172-19179.
35. H. L. Du, J. Y. Li, J. Zhang, G. Su, X. Y. Li and Y. L. Zhao, *J. Phys. Chem. C*, 2011, **115**, 23261-23266.
36. H. Sun, *J. Phys. Chem. B*, 1998, **102**, 7338-7364.
37. H. Z. Wu, L. M. Liu and S. J. Zhao, *Phys .Chem. Chem. Phys.*, 2014, **16**, 3299-3304.
38. F. Li, Y. Qu and M. Zhao, *Carbon*, 2015, **95**, 51-57.
39. Y. Jiao, A. Du, S. C. Smith, Z. Zhu and S. Z. Qiao, *J. Mater. Chem. A*, 2015, **3**, 6767-6771.

40. W. Hu, X. Wu, Z. Li and J. Yang, *Phys. Chem. Chem. Phys.*, 2013, **15**, 5753-5757.
41. S. Blankenburg, M. Bieri, R. Fasel, K. Mullen, C. A. Pignedoli and D. Passerone, *Small*, 2010, **6**, 2266-2271.
42. Z. Zhu, *J. Membr. Sci.*, 2006, **281**, 754-756.
43. M. Shan, Q. Xue, N. Jing, C. Ling, T. Zhang, Z. Yan and J. Zheng, *Nanoscale*, 2012, **4**, 5477-5482.
44. T. Wu, Q. Xue, C. Ling, M. Shan, Z. Liu, Y. Tao and X. Li, *J Phys Chem C*, 2014, **118**, 7369-7376.

Table of Content (TOC)

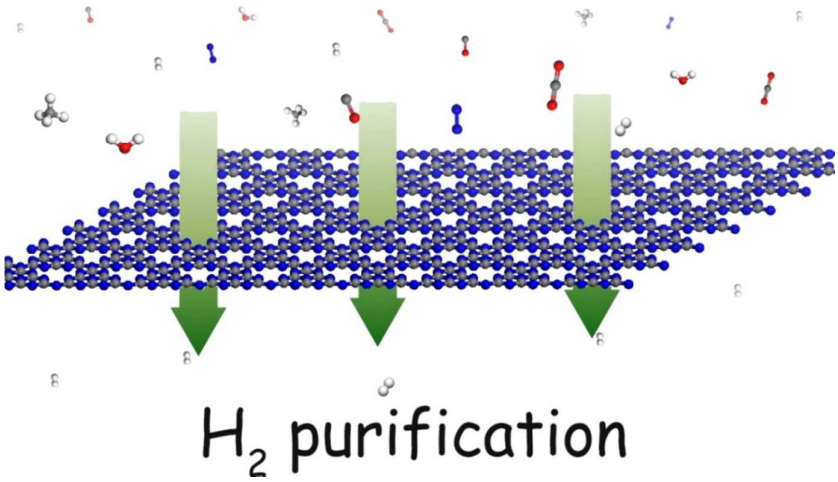

Graphitic C_3N_4 nanosheet with well-ordered sized intrinsic vacancy provides a natural porous diffusion pathway to separate H_2 from the common gases.